Journal of Non-Newtonian Fluid Mechanics 277 (2020) 104236

Contents lists available at ScienceDirect

Journal of Non-Newtonian Fluid Mechanics

journal homepage: www.elsevier.com/locate/jnnfm

Estimation of shear rate change in vertically oscillating non-Newtonian fluids: Predictions on particle settling

Maduranga Amaratunga*, Herimonja A. Rabenjafimanantsoa, Rune W. Time

Department of Energy and Petroleum Engineering, University of Stavanger, Norway

ARTICLE INFO

Keywords:
Oscillatory motion
Shear viscosity
Shear rate change
Non-Newtonian fluids
Particle settling

ABSTRACT

This study investigates the effect of oscillatory motion on velocity and shear rate change within different non-Newtonian, slightly viscoelastic fluids oscillated in a vertical U-shaped circular pipe. An estimation to quantify the influence on particle settling in an oscillatory environment is also presented. Flow visualization using particle image velocimetry (PIV) technique was deployed to compare the two-dimensional velocity field in the vertical plane of the U-tube axis and the resulting shear rate change in three different non-Newtonian fluids. The experiments were performed in a 1.2 m high, 50 mm diameter transparent test section, at room temperature (21 ± 0.5 °C) and atmospheric pressure.

A piston was driven at harmonic motion via a gas buffer, to provide the driving force for the test fluids at four different low frequencies ranging from 0.1 – 0.75 Hz and at three different piston oscillation amplitude ratios of $A = a/D = 0.3$, 0.4 and 0.5, where a is the displacement amplitude of the piston and D is the pipe diameter. Oscillatory Reynolds number (Re_δ) based on Stokes layer thickness was used as the criteria for determining the specific flow regime. 36 different experimental cases were tested within the range of $2 < Re_\delta < 34$, and all the experimental cases exhibited the laminar flow regime.

The study reveals that the axial velocity amplitude along the pipe centerline increases with the increasing frequency and with increasing oscillation amplitude irrespective of the non-Newtonian fluid type. The thickness of the shear region decreases with the increase of frequency. The change of shear rate is maximum near the wall region of the pipe and that is achieved at the maximum position of the phase cycle, where the axial velocity also possesses its highest magnitude. The most viscous and the least elastic fluid have reported a maximum reduction of viscosity as an effect of the oscillatory motion and the viscosity reduction becomes insignificant when the non-Newtonian fluids become less viscous.

1. Introduction

Oscillating flow is a special case of pulsatile flow where, the velocity of the flow is varied with time and there is no steady velocity superposed on that [1,2]. Harmonic oscillating flow is the most simple unsteady flow [3] and similar to fully-developed pipe flow, the oscillatory flow in pipes can also be either laminar, transitional or turbulent [4–6]. In industrial applications, the occurrence of any oscillatory motion within a pipe can be characterized as a cause-and-effect relationship where both ways are possible: system vibrations and noise themselves can cause flow oscillations while the flow pulsations can appear in the mode of self-oscillations due to unattenuated local fluctuations.

Many applications can be found where the oscillatory motion and self-induced vibrations could be identified such as blood flow in the large arteries [7], respiratory flow in the trachea [1], oil pressure engineering, reciprocating compressors, gas kicks and pressure oscillations in oil well drilling [8], food transportation [9], etc. Furthermore, oscillatory motion is employed deliberately in many applications such as solid control techniques, situations where an enhancement of heat and mass transfer is expected [10], for stimulation of oil reservoirs [11], design of pumps and other process equipment with transient flow patterns and for treatment of groundwater aquifers contaminated by organic liquids [12], etc.

1.1. Past work regarding the oscillatory flow

Many researchers have investigated this unsteady, oscillatory flows in horizontal ducts and pipes. However, the majority of those studies are hydrodynamic flow regime testing experiments for Newtonian fluids [1,2,5,6,13–17], where they mostly talk about the transition from laminar to turbulent flow regime. In addition to these, Iguchi et al. [14] have considered a free oscillating flow of a viscous Newtonian fluid in a U-shaped tube and developed an analytical representation for the wall shear stress for the case of laminar flow. However, a significant con-

* Corresponding author.
E-mail address: amaratunga.maduranga@uis.no (M. Amaratunga).

https://doi.org/10.1016/j.jnnfm.2020.104236
Received 20 July 2019; Received in revised form 29 November 2019; Accepted 9 January 2020
Available online 22 January 2020

Notations

CMC	Carboxymethyl Cellulose
CLAHE	contrast limited adaptive histogram equalization
DPIV	digital particle image velocimetry
LVE	linear viscoelastic range
NNF	non-Newtonian fluid
PAC	poly-anionic Celluloselulose
PIV	particle image velocimetry
PIVlab	software tool developed in MATLAB to perform PIV analysis
PL	power-law rheological model
ROI	region of interest
SAOS	small amplitude oscillation shear
a	displacement amplitude
A	amplitude ratio based on the displacement amplitude of the piston
D	diameter of the pipe
De	Deborah number
f	frequency of oscillation, Hz; $\omega/2\pi$
G'	elastic (or storage) modulus
G''	viscous (or loss) modulus
k	non-dimensional phase position; $\omega t/(\pi/4)$
K	consistency index of the non-Newtonian fluid
n	behavior index for the non-Newtonian fluid
r	radial position
R	radius of the pipe
L	entry length for an oscillatory pipe flow
t	time
t_v	viscous time scale
T	oscillation period
$V(t)$	linear velocity with time in the axial direction at the centerline
$\lvert V\rvert$	velocity amplitude in the axial direction at the centerline, $\lvert V\rvert = \lvert a\rvert\omega$
V_{ave}	cross-sectional average velocity
Re_δ	oscillatory Reynolds number based on stokes layer thickness; $\lvert V\rvert\,\delta/\nu$
Wi	Weissenberg number
Wo	Womersley number

Greek Letters

γ	strain
$\dot{\gamma}$	shear rate
δ	oscillating boundary layer (Stokes layer); $\sqrt{2\nu/\omega}$
δ_{ve}	viscous penetration depth for a viscoelastic fluid
ω	angular frequency; $2\pi f$
ν	kinematic viscosity of the fluid
ϑ	phase shift angle (or loss angle) for the viscoelastic fluid
λ	relaxation time of the viscoelastic non-Newtonian fluid
μ	dynamic viscosity of the fluid
$\lvert\mu^*\rvert$	complex dynamic viscosity
γ_L	limiting value of the shear strain
η	non-dimensional radius; $2r/D$
ρ	density of the fluid
Λ	Stokes parameter
Λ_{ve}	viscoelastic Stokes parameter

tribution could be found in literature where several researchers have employed different non-Newtonian fluids in their studies regarding oscillatory laminar flow. Such studies could be either between infinitely large parallel plates [18] or in a rigid tube of infinite length and circular cross-section [19]. The non-Newtonian fluids used in such studies have different rheological characteristics such as highly viscous and shear-thinning, constant viscosity but elastic (Boger fluids), viscoelastic, etc. For example, Khabakhpasheva et al. [20] have studied the pulsating flow of viscoelastic fluids while Balmer and Florina [21] have studied the same as an inelastic power-law fluid. After the early works of Barnes et al. [22,23] on the effects of pressure gradient oscillations around the non-zero mean in the straight circular pipe, Siginer [24] has provided a very detailed and a comprehensive piece of theoretical work which was useful for the future researchers. Instabilities [25], and nonlinearity [26] have received great attention related to the oscillatory flow of a complex fluid. Theoretical work presented by Rio et al. [27,28] and also the studies on worm-like micellar solutions subjected to pulsating flow [29,30] provide more insight on the oscillatory flow of non-Newtonian fluids in many aspects. Furthermore, the study performed by Mitran et al. [31] on the extensions of the Ferry shear wave model [32,33] and the studies performed by Lindley et al. [34] on the spatial stress and strain distributions of viscoelastic layers in oscillatory shear are also remarkable with this regard. However, the studies on pulsating turbulent flows [35,36] have also become increasingly popular in the recent past.

1.2. Effect of oscillatory motion on non-Newtonian fluids

The oscillatory flow of a non-Newtonian fluid is remarkably different from that of a Newtonian fluid, even at low driving frequencies. Particularly, viscoelastic fluids could exhibit both viscous dissipative behavior of simple fluids and also the elastic response characteristic of solids which originates from the re-orientation and stretching of the fluid molecules. When subjected to oscillatory motion highly viscoelastic non-Newtonian fluids could be resulted in a resonance behavior [37,38] and also with a vortex ring formation [39]. There could be dramatic differences in the dynamic response of a non-Newtonian fluid [27,40–42] compared with Newtonian fluid. As explained in Section 1.1, non-Newtonian fluids that are highly viscoelastic exhibit significant resonance peaks at particular driving frequencies. The shear-induced instabilities in nonlinear complex (viscoelastic) fluids lead to the formation of complex non-symmetric structures by making the vortex structures more unstable at higher driving frequencies and amplitudes. This type of formation of vortex structures or resonance behavior of viscoelastic oscillatory pipe flow systems is highly noticeable in comparison with the purely dissipative response of a Newtonian fluid in the same experimental conditions.

Furthermore, oscillatory motion naturally leads shear-thinning non-Newtonian fluids to experience shear rate related changes in rheological parameters such as shear viscosity, gel formation and extensional viscosity [43], etc. For example, in the drilling industry, the use of primary solids control devices such as shakers leads to an alteration of the rheological properties of the drilling fluids [44]. Most of the water-based drilling fluids usually have a strong gel structure since they possess a high extensional viscosity. According to Saasen and Hodne [44,45], such drilling fluids having high extensional viscosity are generally not that affected by vibrations/oscillations. Furthermore, they explain that oil-based drilling fluids are much more sensitive to the oscillatory effects than water-based drilling fluids. In the concrete industry, the provision of vibrations with the correct amplitude reduces the viscosity of the cement paste [46]. The reason for this type of viscosity change could be explained using the structural units that contain within the polymeric non-Newtonian fluids [47]. These structural units are local agglomerations of particles and polymers that form the viscosity of the fluid. The agglomerations are usually stabilized by the interaction of surface charges of the different particles and when any vibrational field is applied to the fluid, these structural units are partially destroyed and the viscosity is altered.

1.3. Governing non-dimensional parameters for an oscillatory flow

A number of relevant dimensionless parameters that characterize the oscillatory flow at a given driving frequency and amplitude are reported here.

1.3.1. Oscillating Reynolds number (Re_δ)

Many researchers have discussed the extent of laminar to turbulent transition in oscillatory flows [5,15,16,48] with the use of the critical value of oscillatory Reynolds number [1,4–6,14,49] mainly for the Newtonian fluids. The Reynolds number measures the ratio of inertial forces to viscous forces where the oscillating Reynolds number (Re_δ) based on the Stokes boundary layer thickness (δ) is [1,50];

$$Re_\delta = \frac{|V|\delta}{\nu} \tag{1}$$

Here, $|V| = |a|\omega$ is the amplitude of the centerline velocity in the axial direction, a is the displacement amplitude, $\omega = 2\pi f$, where f is the frequency of oscillation and ν is the kinematic viscosity of the fluid concerning within the circular pipe. This Stokes boundary layer or the viscous penetration depth is defined as [1];

$$\delta = \sqrt{\frac{2\nu}{\omega}} \tag{2}$$

It is to be noted that, δ is particularly defined for a Newtonian fluid where transverse oscillations are therefore overdamped (cannot propagate into the fluid). However, since things are different for viscoelastic non-Newtonian fluids, this special notion has been successfully extended to adapt for the simplest viscoelastic fluid (a Maxwell fluid) as described in Section 1.3.4.

In literature, different researchers have used different terminology to define this oscillatory Reynolds number [4,20,25,51] and thus the critical value where the transition from laminar to turbulent flow takes place. Taking into consideration all the different literature vales, authors have concluded that, $Re_\delta = 500$ (based on viscoelastic Stokes boundary layer which will be defined later in this paper) is to be considered as the critical Reynolds number for this study of oscillatory flow in a vertical pipe. The evaluation of the Reynolds number for the different cases of this study is mentioned under Section 3.2.1.

1.3.2. Womersley number (Wo)

It is a measure of the ratio of the pipe radius to the distance through which vorticity diffuses away from the wall in one period of oscillation [52]. It was introduced by Womersley [53]. It is the basic parameter of an oscillatory flow (sometimes referred to as the "non-dimensional frequency" [13,52] and can be expressed as [48];

$$Wo = \frac{D/2}{\sqrt{\nu/\omega}} \tag{3}$$

It is claimed that increasing (Wo) should lead to a stable state of the flow if Re_δ is held constant [1].

1.3.3. Stokes parameter (Λ)

The Stokes parameter measures the ratio of the pipe radius ($R = D/2$) to the viscous penetration depth (δ) for oscillatory viscous flow in a pipe. Thus, Λ can be expressed as [2,5];

$$\Lambda = \frac{D/2}{\delta} = \frac{D}{2}\sqrt{\frac{\omega}{2\nu}} \tag{4}$$

Here, Λ is defined based on δ for a Newtonian fluid and relevant adaptations for a non-Newtonian fluid are explained in Section 1.3.4.

1.3.4. Deborah number (De)

This is one of the main dimensionless parameters to describe the flow of any non-Newtonian viscoelastic fluid. For a simple viscoelastic fluid (a Maxwell fluid), since the stress relaxation can be described by a single time constant which we call the relaxation time (λ) of the fluid, it has been employed in defining the non-dimensional parameters related to non-Newtonian oscillatory flows. De is the measure of the relative importance of the relaxation time (λ) of any viscoelastic fluid to the scale of the flow which is the same as the characteristic time or the oscillation period ($T = \frac{2\pi}{\omega}$) for the deformation process [54]. De can be expressed as;

$$De = \frac{2\pi\lambda}{T} = \lambda\omega \tag{5}$$

As explained in Section 1.3.1, since the behavior of non-Newtonian fluids are different from that of simple dissipative Newtonian fluids, the viscous penetration depth for a viscoelastic fluid (δ_{ve}) is expressed as [55];

$$\delta_{ve} = \delta\left(De + \sqrt{1 + De^2}\right) \tag{6}$$

It is clear that the difference between Eqs. (2) and (6) is imposed by the elasticity of the fluid ($De > 0$), so that the transverse oscillations can effectively propagate before they are attenuated.

Furthermore, the viscoelastic Stokes parameter (Λ_{ve}) can be expressed as [55];

$$\Lambda_{ve} = \frac{R}{\delta} \tag{7}$$

In analogy to Λ, the parameter Λ_{ve} is the ratio of the radius to the extension of the shear waves generated by the pipe walls. In the theoretical analysis performed on the laminar oscillatory flow of Maxwell and Oldroyd-B fluids, Casanellas and Ortin [55] characterize the non-Newtonian oscillatory systems into two main categories as; (1) 'narrow' systems for $\Lambda_{ve} < 1$, when viscoelastic shear waves extend through the whole system and (2) 'wide' systems for $\Lambda_{ve} > 1$, when an inviscid core is present at the center of the pipe.

1.3.5. Viscous to relaxation time ratio

This is another important non-dimensional parameter that characterizes the flow of any non-Newtonian viscoelastic fluid. The viscous time scale (t_v) to relaxation time ratio is expressed as;

$$\text{Viscous to relaxation time ratio} = \frac{t_v}{\lambda} = \frac{R^2/\nu}{\lambda} \tag{8}$$

Following a similar characterization method, Casanellas and Ortin [55] state that, at $t_v/\lambda << 1$ (where highly viscoelastic fluids are oscillated in narrow tubes) the resonant behavior could occur. At $t_v/\lambda = 1$ the velocity magnitude at the center is strongly decreased and for $t_v/\lambda >> 1$ the resonances could completely disappear.

1.3.6. Weissenberg number (Wi)

The ratio of the relaxation time of the fluid to the characteristic inverse shear rate is defined as the Weissenberg number. Wi is expressed as [54];

$$Wi = \lambda\dot{\gamma} \tag{9}$$

Here, $\dot{\gamma}$ is the shear rate and can be calculated as is the relative velocity of two fluid layers moving with respect to each other [56,57] and is expressed as;

$$\dot{\gamma} = \frac{dV}{dr} \tag{10}$$

where, r denotes the radial distance. A value of higher Wi indicates the elastic stresses become large and the onset of elastic instabilities.

1.4. Measurements using PIV technique

Particle image velocimetry (PIV) technique is a non-intrusive optical technique, which has been used widely in literature to visualize the two-dimensional velocity distributions [58]. The non-intrusivity of the PIV technique is important in investigating scientific and engineering applications when it is necessary to avoid disturbances to the flow itself. Even though PIV has been employed in the measurement of single-phase flows in many research studies since the 1970s, it has only recently been applied in oscillatory flows [25,50]. Trip et al. [17] have utilized the PIV technique extensively to investigate how the critical Reynolds number is affected by different pulsatile conditions in horizontal pipe flow and on

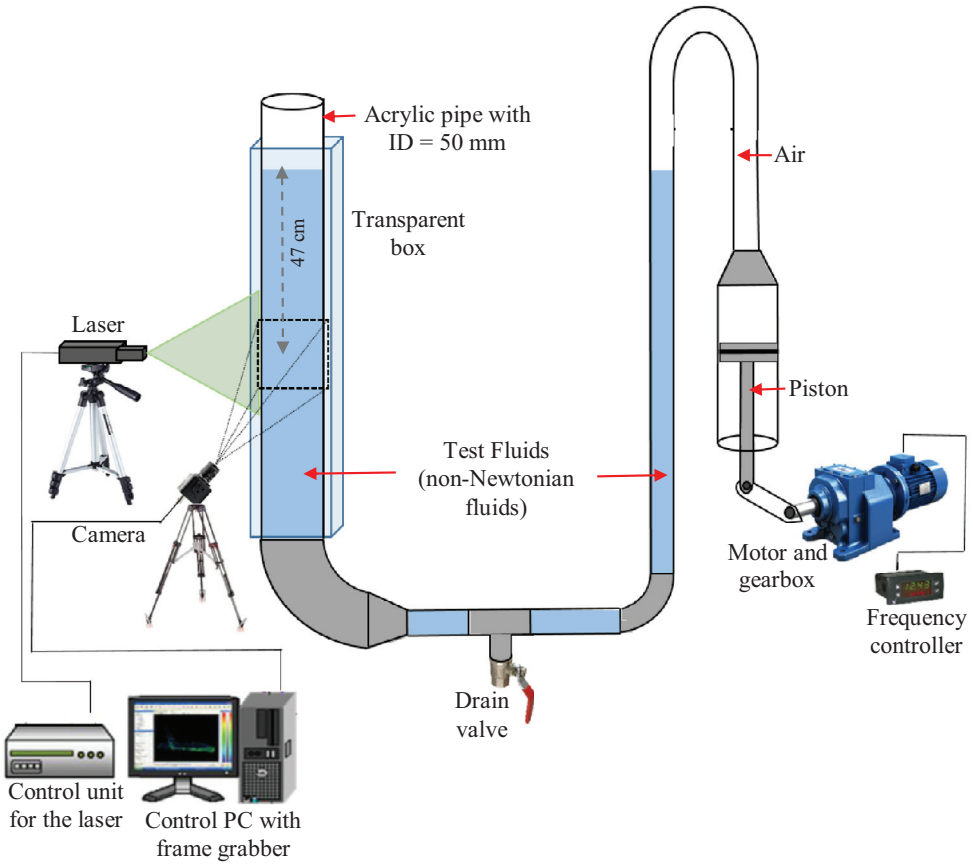

Fig. 1. Sketch of the experimental setup.

the transition to turbulence. Based on the experimental study performed by Amaratunga et al. [57] on the horizontal oscillatory motion of a fluid medium in a vertical rectangular column, the influence of oscillatory motion on the dynamic velocity profiles in non-Newtonian drilling fluids is discussed together with the influence on particle settling. The PIV technique has been used by Blythman et al. [59] to characterize the dependence of wall shear stress and pressure gradient with frequency for oscillatory flow in a two-dimensional rectangular channel. The study performed by Torralba et al. [42] using PIV to present dynamic velocity profiles in a Newtonian and a viscoelastic Maxwell fluid driven by an oscillating pressure gradient in a vertical cylindrical pipe seems to render some valuable input for this current investigation.

1.5. Objective and scope of the study

It has been identified that the free oscillating flow in a U-shaped tube is a fundamental and generic flow setup to study the various types of unsteady motion of fluids [14]. However, the present study is employed with a piston-driven forced oscillation having the objective of obtaining a better visual picture of the phenomena occurring in oscillatory flow in a vertical pipe system.

There are several studies in the literature that depicts the macroscopic manifestations, such as the changes in flow properties flow enhancements [60], etc. impacted by vibrations and oscillations on non-Newtonian liquids. However, neither the effect of oscillatory flow on non-Newtonian fluid rheology nor the impact on particle settling is fully understood in highly reversed flows like those investigated in this study. This paper focuses on utilizing PIV to visualize the oscillatory flow in a more quantitative and systematic manner. It describes how the shear-thinning non-Newtonian drilling fluid rheological properties alter when they are exposed to oscillatory motion within a pipeline and predicts the consequences on particle settling. This investigation is partly motivated by challenges associated with operational procedures during drilling and maintenance of petroleum wells and it is also part of a comprehensive study aimed at investigating the influence of low-frequency oscillations on particle settling in non-Newtonian drilling fluids.

2. Methodology

The experiments were performed in the multi-phase flow laboratory at the University of Stavanger (UiS), Norway.

2.1. Experimental set up

Fig. 1 shows a sketch of the U-shaped experimental set up used for the investigation of the effect of low-frequency oscillatory motion on non-Newtonian fluids. The test section on the left limb of the U-tube has a circular cross-section with an internal diameter of 50 mm and a total length of 1200 mm. The bottom and the right limbs of the U-tube were also circular in cross-section and 30 mm in internal diameter. The whole U-tube including the piston cylinder (with an internal diameter of 50 mm) was made of transparent acrylic for visualization purposes.

Harmonic oscillations were provided by the piston attached to the right limb of the U-tube, which is driven by a motor-gearbox unit. The rotary motion of the gearbox is converted to a reciprocating motion of the piston by mechanically projecting it into the arm of the piston. The revolution speed of the motor (model: 3DF56-2S7032 from ABM Greiffenberger, Germany) and the gearbox from David Brown (Radicon series), UK was controlled by a frequency controller (model: Micromaster 420 from Siemens) in such a way that the required output frequency was set to the piston. A tachometer (model: AT-6 L from Clas Ohlson, Norway) was used to confirm the frequency of the piston. Experiments with four different oscillation frequencies were tested as 0.1, 0.25, 0.5 and 0.75 Hz. Several combinations of the length of the rotating arm allowed

Table 1
Specific details of the polymers and the mixture configuration.

Polymer type	Viscosity at 25 °C	Used weight (g) to dissolve in 5 L of deionized water		
		Fluid 1	Fluid 2	Fluid 3
PolyPAC	800–1200 mPa.s (1% H_2O)	0.5	5	4.5
MV-CMC	400–1000 mPa.s (2% H_2O)	7.5	5	7.5
HV-CMC	1500–3000 mPa.s (1% H_2O)	22.5	5	2.5

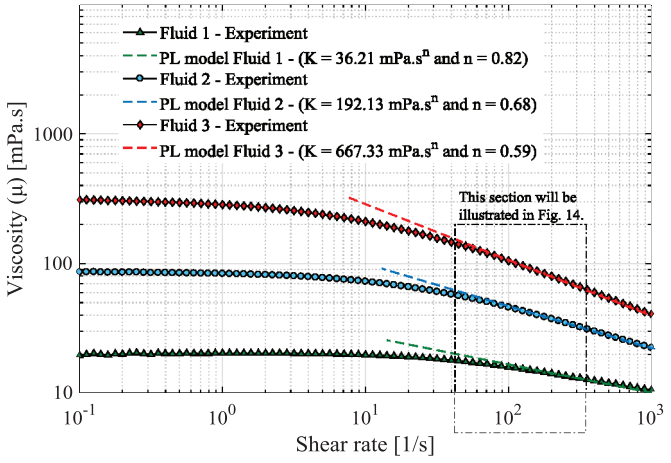

Fig. 2. Viscosity curves for the test fluids at 21 °C.

the oscillating amplitude to be varied as 15, 20 and 25 mm. Out of that, the oscillation amplitude ratio (A) was determined as $a/D = 0.3$, 0.4 and 0.5, where a is the displacement amplitude of the piston and D is the pipe diameter. In order to avoid optical aberrations, the test section was placed inside a second recipient of transparent acrylic, of square cross-section (15 × 15 cm^3), filled with the same deionized water to match the refractive index of the acrylic walls.

2.2. Materials and fluids

Deionized water was used to prepare three polymeric non-Newtonian Fluids (NNF), later referred to as "Fluid 1", "Fluid 2" and "Fluid 3". They are a mixture of three water-based polymers namely Poly-anionic Cellulose (PAC) called PolyPAC-R provided by MI-Swaco, Norway, medium viscous Carboxymethyl Cellulose (MV-CMC) and high viscous Carboxymethyl Cellulose (HV-CMC) provided by Sigma-Aldrich. The specific details of the polymers and the mixture configuration are mentioned in Table 1.

The viscosity of the NNF was measured by Anton Paar MCR 302 rotational rheometer and the rheological properties are described in Section 3.1 with Fig. 2. The density values of the fluids measured using Anton Paar DMA-4500 density meter were 998.26, 999.01 and 1000.13 kg/m^3 for Fluid 1, Fluid 2 and Fluid 3, respectively. All experiments were carried out and liquid properties were measured at room temperature of 21 ± 0.5 °C and atmospheric pressure. Based on these variables, 36 different experimental cases were tested within the range of $2 < Re_\delta < 34$ as shown in Table 2. All the non-Newtonian fluids were assumed to be incompressible.

2.3. The PIV system

2D PIV technique was employed in measuring the velocity fields in a vertical plane, along the symmetry axis of the test limb of the U-tube. The measurement area for the PIV system was centered at 470 mm below the equilibrium air-liquid interface (see Fig. 1), so that the end-effects from the free surface and the bend of the U-tube was minimized.

Table 2
Test matrix.

State variable	Range and unit
Test Fluids	Fluid 1, Fluid 2 and Fluid 3
Oscillation frequencies (f)	0.1, 0.25, 0.5 and 0.75 Hz
Oscillation amplitude ratio (A)	0.3, 0.4 and 0.5 (-)
Measured variables	Velocity from PIV

Replacing δ by δ_{ve} accordingly, the present experimental set up has provided sufficient entry lengths from both sides as explained by Gerrard and Hughes [52] and Yamanaka et al. [3] for Newtonian fluids, which is $L = 0.3\ \delta Re_\delta$, where L is meant to be the entry length for an oscillatory pipe flow. A Basler camera (Model: acA800-510um USB 3.0 camera with the ON Semiconductor) with a maximum frame rate of 500 fps at full resolution of 800 × 600 $pixel^2$ was used for the acquisition of images. The images for the PIV analysis were acquired at 200 fps by the camera that was equipped with a Nikon AF Nikkor 50 mm – f/1.4D lens. The images were cropped to a reduced section of 560 × 460 $pixel^2$ to fit the view of interest. The measurement area of the PIV system was illuminated with a Photop LDC-2500S continuous-wave laser (class 3B) at wavelength 532 nm (green light spectrum) and variable output up to 200 mW. The thickness of the laser beam was set to approximately 1 mm using a lens and the collimator system. The laser sheet was aligned such that it illuminates the vertical plane through the center of the pipe (see Fig. 1). In order to illuminate the fluid motion, Polyamide seeding particles were used (Model: PSP50, Dantec Dynamics), with mean particle diameter = 50 μm and specific density = 1.03 g/m^3 as the tracer particles. The Stokes number (Stk) for the seeding particles were approximately $5.5 \times 10^{-4} \ll 0.1$ and the settling speed of the seeding particles are very small, typically less than 10^{-7} m/s. The change of rheology of the test fluids due to the addition of seeding is negligible. The results were acquired after allowing the system to oscillate at least for 1 min to achieve a stable periodic motion up and down.

2.3.1. Data treatment and analysis

The PIV analysis was performed using PIVlab – version 2.01 [61], which is a digital particle image velocimetry (DPIV) tool developed in MATLAB. A region of interest (ROI) that was limited to the pipe cross-section rather than the entire image was selected. Also, the size of the smallest interrogation area for the present analysis was selected as 16 × 8 pixels based on the guidelines provided by Jensen [62]. All the images were pre-processed using contrast limited adaptive histogram equalization (CLAHE) method and some of the background noise was removed using high-pass filter. For the PIV settings, a FFT window deformation was adopted as explained by Thielicke and Stamhuis [61]. The axial velocity component of the vertically oscillating fluid medium along the centerline of the pipe and along the diameter of the pipe was distinguished separately from the velocity magnitudes obtained from PIV analysis for further processing.

3. Results and discussion

The significance of the different fluids selected for this study in a rheological context is described in the following section. In particular,

Table 3
Rheological parameters for the test fluids.

	K (mPa.s^n)	n (-)	λ (s)
Fluid 1	36.21	0.82	0.037
Fluid 2	192.13	0.68	0.021
Fluid 3	667.33	0.59	0.016

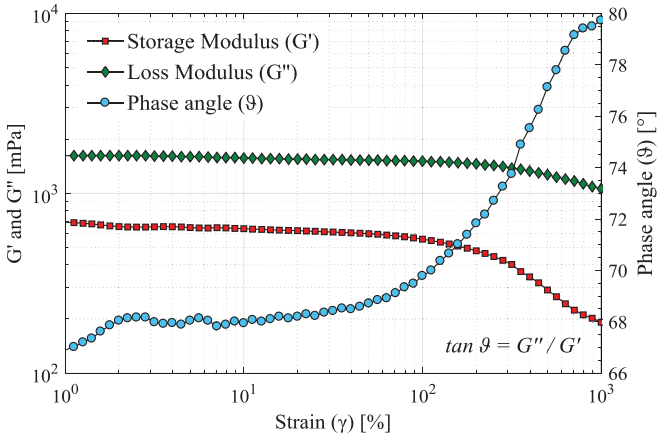

Fig. 3. Amplitude sweep test for Fluid 3 at a constant angular frequency of $\omega = 10$ rad/s.

this regards how local velocity and the corresponding shear rate vary with different oscillatory conditions.

3.1. Rheology of non-Newtonian fluids

The rheological properties of the non-Newtonian fluids were measured by a modular compact rheometer (Anton Paar – MCR 302), using the concentric cylinder configuration (CC27). Fig. 2 shows the dynamic viscosity (μ) curves for the all the three fluids used in the experiment, together with their corresponding power-law parameters. The power-law rheological model was used to model the viscous and the shear-thinning behavior of the test fluids as shown in Eq. (11);

$$\mu_{PL} = K\dot{\gamma}^{n-1} \tag{11}$$

Here, μ_{PL} is the viscosity predicted by the power-law model, K is the consistency index, n is the behavioral index and $\dot{\gamma}$ is the shear rate. The parameters for the model are mentioned in Fig. 2 and also summarized in Table 3.

The shear-thinning behavior of the test fluids can be easily distinguished from the viscosity curves where Fluid 3 is the most shear-thinning fluid with the lowest n value. It is to be noted that, the power-law model has been applied only for the linear region of the experimental viscosity data and that does not cover the constant viscosity plateau observed in the low values of shear rate. The highlighted section will be further illustrated in Fig. 14, in Section 3.4.2.

The viscoelastic properties of the test fluids were also measured in small amplitude oscillation shear (SAOS) tests as part of the rheological investigation. In order to determine the linear viscoelastic (LVE) region at low strain amplitudes, and also to investigate the viscoelastic behavior of the samples, strain amplitude sweeps and frequency sweeps were conducted. Fig. 3 shows the results of the amplitude sweep test only for Fluid 3, over a given strain (γ) range. It was ramped up logarithmically from 1 to 1000%, at a constant angular frequency of $\omega = 10$ rad/s.

It can be observed that the viscous (same as loss) modulus (G'') of Fluid 3 is larger than its elastic (or storage) modulus (G'), and the calculated phase angle (ϑ) is varying from approximately 65° to 80°. The variation of moduli curves for the two other test fluids also shows a similar trend, where there is no crossover point between the moduli curves.

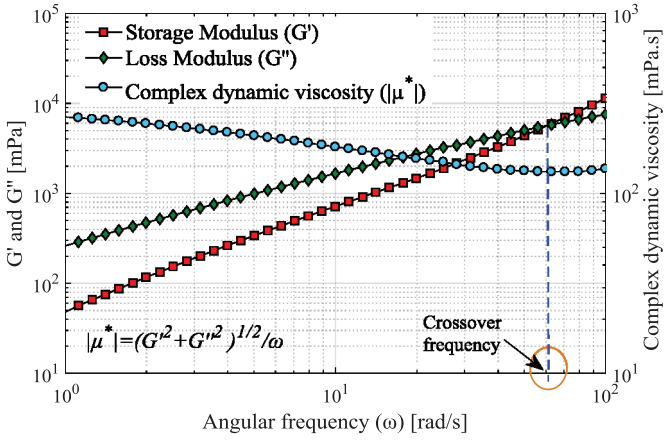

Fig. 4. Frequency sweep test for Fluid 3 at a constant strain at $\gamma = 1\%$.

Therefore, it could be concluded that all three test fluids are slightly viscoelastic at the corresponding low shear region. The G' curve for Fluid 3 starts to lose its plateau value at around 10% of shear strain which corresponds to a shear rate value of $\dot{\gamma} = 1$ 1/s. That is identified as the limiting value of the shear strain (γ_L) for Fluid 3 which defines the LVE range. Other test fluids have shorter LVE ranges than Fluid 3 where Fluid 1 has the shortest with its G' starts to decrease at much lower strain around ($\gamma < 2\%$).

The viscoelastic property of any polymer solution in its LVE range is reflected in the frequency sweep data, which can be used to investigate the time-dependent deformation behavior of any sample. It is a direct measure of elasticity [63]. Fig. 4 shows the results of the frequency sweep test for Fluid 3 over a given angular frequency (ω) range (ramped down logarithmically from 100 to 1 rad/s) at a constant strain 1%.

It can be seen from Fig. 4 that, both the elastic and the viscous moduli increase when the frequency is increased. However, the elastic modulus (G') increases faster than the viscous modulus (G'') and the solid-like behavior of the fluid becomes dominant after the crossover frequency as illustrated in Fig. 4. The inverse of this crossover frequency represents the longest characteristic relaxation time (λ) of the polymer solution [64] and the corresponding λ values for the three fluids are mentioned in Table 3. According to the values presented in Table 3, it can be observed that Fluid 1 has the highest relaxation time of the test fluids and therefore has the highest elasticity. Since the λ values are very small, it could be concluded that the test fluids are only slightly viscoelastic. All the aforementioned rheological properties were measured just after the corresponding experimental run.

3.2. Axial velocity variation at the pipe centerline

The characteristic driving sinusoidal harmonic motion was identified by determining the axial velocity along the centerline of the pipe. The centerline is the best location to identify the maximum up and down motion of the fluid with the least possible viscous and wall effects. Fig. 5 presents the axial velocity profiles of Fluid 1 and 2, along the pipe centerline when they are oscillated at a frequency of 0.75 Hz and at a piston amplitude ratio (defined previously) of $A = 0.5$. The axial velocity at the pipe centerline shown in Fig. 5 is used as a basis to introduce the notation system adopted by the authors to discuss the results in the latter part of this paper.

The phase position/angle (ωt) was made dimensionless using the angle value ($\pi/4$), and the value for $\omega t/(\pi/4)$ has been utilized in presenting and discussing further results. Qualitatively, the periodical shape of the curves obtained from the PIV measurements confirms the successful transmission of energy from the mechanical piston to the fluid system via the gas buffer in between them. The quantitative description of the

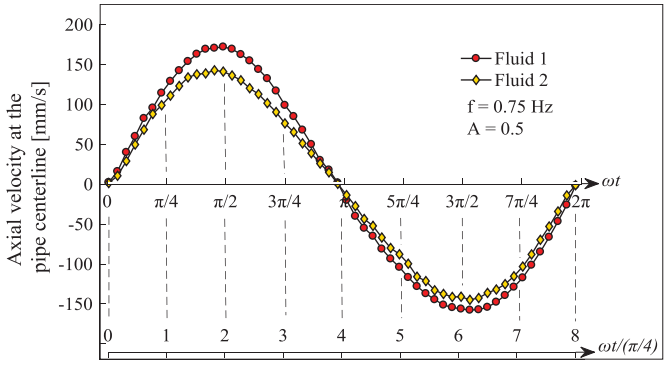

Fig. 5. Introduction of the different phase positions within the phase cycle based on centerline axial velocity.

Table 4
De for the test fluids and different driving frequencies.

	f_1	f_2	f_3	f_4
F 1	0.0229	0.0575	0.1149	0.1724
F 2	0.0132	0.0329	0.0658	0.0987
F 3	0.0103	0.0258	0.0517	0.0775

*F 1, F 2 and F 3 represent Fluid 1, Fluid 2 and Fluid 3 respectively. f_1, f_2, f_3 and f_4 represent the frequency values of 0.1 Hz, 0.25 Hz, 0.5 Hz and 0.75 Hz, respectively.

different velocity curves plotted in Fig. 5 is provided in Section 3.2.3. However, the asymmetry of the axial velocity between the first and second half of the cycle for Fluid 1 demonstrates some local friction exerted on the piston motion especially on its decelerating phase.

3.2.1. Evaluation of the flow field associated with the experiments

Based on the rheological characterization provided in Section 3.1, the test fluids are slightly viscoelastic and show power-law characteristics in their linear region. First, they are evaluated for their De ($= \lambda\omega$) based on the oscillation frequency and values are reported in Table 4.

All the values for the calculated De are less than unity and not large enough for resonances to occur [25]. According to Casanellas and Ortin [55], these small De make the attenuation length of the viscoelastic waves essentially identical to their wavelength and the oscillating boundary layer of these fluids could be mostly similar to that of a Newtonian case without resonances.

In addition to De, it is useful to evaluate the viscoelastic Stokes parameter (Λ_{ve}) for the experimental cases to get a better understanding of the oscillating system in concern. According to Eq. (6), it can be easily understood that the viscous penetration depth for viscoelastic fluids is greater than that of Newtonian fluids because of the presence of relaxation time (λ) in viscoelastic fluids. To illustrate the difference, we consider the ratio of Stoke parameters for both Newtonian and viscoelastic fluids as;

$$\frac{\Lambda}{\Lambda_{ve}} = \frac{R/\delta}{R/\delta_{ve}} = \frac{\delta_{ve}}{\delta} \tag{12}$$

and Fig. 6 shows a plot of δ_{ve}/δ as a function of De for the driving frequencies and test fluids concerned within this study.

According to Fig. 6, it can be seen that δ_{ve}/δ (similar Λ/Λ_{ve}) is increasing linearly with De and is always greater than unity for all the driving frequencies of this study. It confirms the fact depicted by Eq. (6) also that the viscous penetration depth for viscoelastic fluids is greater than that of Newtonian fluids because of the presence of relaxation time in viscoelastic fluids. Since the test fluids concerned within this study are slightly viscoelastic, it can be seen that δ_{ve}/δ is just over unity, but still it is increasing with De. However, since $\Lambda_{ve} > 1$ for all the test cases, the system could be considered as a 'wide' system according to Casanellas and Ortin [55].

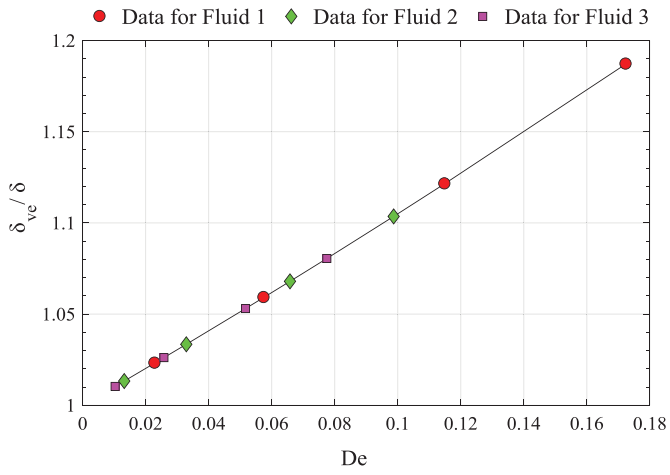

Fig. 6. Variation of δ_{ve} with respective to δ at different De.

Furthermore, with the introduction of experimental setup length (which is the pipe radius in our case), the ratio of viscous time scale to the relaxation time scale (t_v/λ) is calculated for further characterization of the experimental system. Fig. 2 showed that all the test fluids are shear-thinning non-Newtonian fluids and they have a shear rate dependent viscosity. Since $\dot{\gamma} = 100$ 1/s represents the shear rate value within a typical drilling pipe [65], the shear viscosity value of each test fluid corresponding to $\dot{\gamma} = 100$ 1/s has been utilized in the calculation of t_v/λ. For the test fluids and conditions considered, the ratio of viscous to relaxation time yields 1072.8 for Fluid 1, 646.9 for Fluid 2 and 361.9 for Fluid 3, which are greatly larger than the unity. Therefore, the possibilities of occurring resonance are disappeared while the system can be considered as a 'wide' system where the oscillation takes place comparably in a large geometry ($D = 50$ mm) and the flow in the central core could be inviscid [55].

However, the differences in piston driving amplitude and the consequences of that were not taken into account in the above non-dimensional parameter evaluations. Therefore, in order to identify the flow features more precisely, it is important to determine the correct hydrodynamic flow regime which each experimental case belongs to. Table 5 reports the Reynolds number values for all the experimental cases of this study. The oscillating Reynolds number (Re_δ) based on viscoelastic Stokes boundary layer (δ_{ve}) is used for this determination as depicted by Eq. (6). Similar to that used in t_v/λ calculation, the shear viscosity value of each test fluid corresponding to $\dot{\gamma} = 100$ 1/s was employed. Further, the maximum velocity amplitude values reported in Section 3.2.3 have been utilized for the calculations.

It is to be noted that the calculated Re_δ is based on the PIV measurements performed through the fixed observation window centered 470 mm below the equilibrium air-liquid interface (see Fig. 1). This is the optimal location in the vertical test section to minimize the end and entrance effects in the pipe. According to Torralba et al. [42], Re_δ could have been even lower if the measurement was carried out closer to the air-liquid interface. Therefore, based on these calculations, it can be concluded that all the experimental cases belong to the laminar regime and also the nonlinearities of the oscillating flow is due to the rheological properties of the fluids and not due to the inertial effects. Even if the decrease in viscosity due to the shear-thinning is considered, they are well within the laminar regime.

3.2.2. Temporal evolution of the axial velocity distribution along the pipe diameter

The primary data for PIV measurements in the form of instantaneous velocity fields for some specific positions of the phase cycle are presented in Fig. 7. It is to be highlighted that, the velocity profiles are drawn based on the centerline axial velocities of Fluid 2 only which is

Table 5
Oscillating Reynolds number (Re_δ) values for all the experimental cases.

	A_1				A_2				A_3			
	f_1	f_2	f_3	f_4	f_1	f_2	f_3	f_4	f_1	f_2	f_3	f_4
F 1	5.27	9.52	14.93	20.31	6.95	12.45	19.99	27.18	9.52	15.56	23.23	33.06
F 2	2.99	5.39	7.45	10.46	4.29	6.98	10.17	14.04	4.39	7.23	11.99	15.12
F 3	–	2.91	4.73	6.202	2.47	3.94	6.25	8.330	2.76	4.26	8.80	11.12

*F 1, F 2 and F 3 represent Fluid 1, Fluid 2 and Fluid 3 respectively. f_1, f_2, f_3 and f_4 represent the frequency values of 0.1 Hz, 0.25 Hz, 0.5 Hz and 0.75 Hz, respectively. A_1, A_2 and A_3 represent the amplitude ratio values of 0.3, 0.4 and 0.5, respectively.

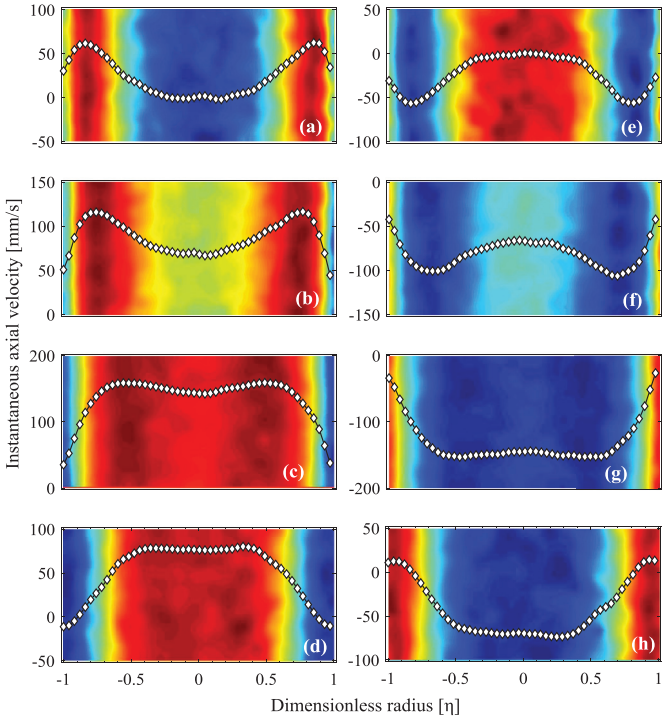

Fig. 7. Instantaneous axial velocity distribution profiles of Fluid 2 with time and phase position at $f = 0.75$ Hz and $A = 0.5$ (a) $k = 0$; (b) $k = 1$; (c) $k = 2$; (d) $k = 3$; (e) $k = 4$; (f) $k = 5$; (g) $k = 6$; (h) $k = 7$ (* The color scale for each subfigure is defined by the magnitude of each plot itself – vertical axis).

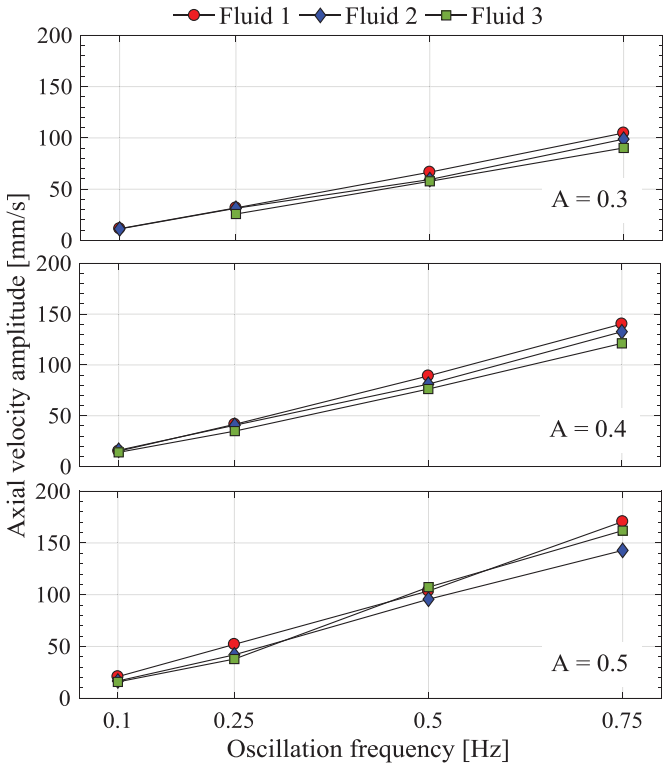

Fig. 8. Axial velocity amplitude variation with different non-Newtonian fluids for different piston amplitude ratios.

oscillated at $f = 0.75$ Hz and $A = 0.5$. The non-dimensional phase position $\omega t/(\pi/4)$ has been denoted as k in the figure caption.

The presented axial velocity profiles seem to be somewhat irregular in shape but almost symmetrical along the pipe centerline. For a fully established steady-state laminar flow, the profile would be parabolic throughout the whole pipe cross-section. However, due to the continuing oscillations and also the highly reversing nature of the flow in the present study, the velocity profile is deviated from the parabolic shape in most of the phase positions and at certain instants with minor similarities to a parabolic shape in the core region of the pipe. At the stage of flow reversal it was observed that while the net axial velocity profile remains positive in the core region, some part of the velocity profile seems to be negative (returns) in a very small region near the wall. This is basically due to the complex structure of the non-Newtonian fluids and even though they are only slightly viscoelastic, they exhibit annular regions within the pipe with alternating upward/downward motion. The thickness of this shear region decreases with increasing frequency. The axial velocity in the shear region either lags or leads the axial velocity in the central region by a small amount, which tends to zero at certain positions of the phase cycle.

As expected, the centerline axial velocity varies periodically in magnitude and direction following the pattern of the imposed oscillations. At higher frequencies, there is an extensive region in the center of the fully developed flow in which vorticity is very small, that is, where the velocity is almost independent of the radial position. The color theme used in the background of the PIV image shown in Fig. 7 illustrates this significance of shear forces. For the non-Newtonian fluid where the effect of wall shear is propagating towards the central axis of the pipe and as a result, different color regions have appeared. However, it is somewhat deviating from the theoretical idea presented in Section 1.3.4 for the system to be 'wide' and the flow in the central core is inviscid. This deviation could be attributed to the highly reversing nature of the system and also to the presence of a compressible air pocket in between the fluid and piston arrangement.

It could be seen from Fig. 7(c) and (g) that, when the piston is at its equilibrium position (where the flow velocity is maximum or minimum), the flow velocity outside the Stokes layer has a Poiseuille velocity profile with different peak velocity magnitudes depending on the frequency.

3.2.3. *Velocity amplitude variation based on centerline axial velocity*

Since Fig. 7 shows the radial velocity variation only for a single experimental case, it is important to investigate how the amplitude of velocity is varying in non-Newtonian fluids with different n values (or polymer concentrations) and with different oscillatory conditions. Fig. 8

compares the velocity amplitude achieved by the liquid medium (at the location of PIV measurements) for different frequencies and at different piston displacement amplitudes. Furthermore, it depicts the impact of the different non-Newtonian fluids on the velocity amplitude.

According to Fig. 8, it can be clearly seen that the axial velocity amplitude along the centerline of the pipe increases with the increasing frequency irrespective of the displacement amplitude of the piston and the fluid type. This can be explained as follows: when the oscillation frequency is increased for fixed piston amplitude, the momentum transfer from the piston to the liquid via the air-buffer is increased and the kinetic energy achieved by the fluid system is also increased. When the kinetic energy of the fluid system is increased, the viscous resistance of the fluid medium reduces and hence the velocity amplitude is increased. A similar scenario could be observed with respect to the displacement amplitude ratios, where the magnitude of the velocity amplitude of the liquid medium increases with increasing piston amplitude ratio.

It is also interesting to see the effect of different shear-thinning non-Newtonian fluids on the nonlinearities of the non-Newtonian liquid medium in terms of the achieved velocity amplitude. It can be observed from Fig. 8 that, when n decreases (or the fluid becomes more viscous) the achieved velocity amplitude of the liquid medium is decreased for a particular piston displacement amplitude ratio and frequency. This situation was visible at all the experimental conditions with a small deviation at $A = 0.5$. This could be attributed to the increased viscous resistance exerted by the non-Newtonian fluids that act as a negative impact on particle settling in drilling fluids by increasing the drag force.

However, to reveal the nonlinearities caused by shear thinning more evident, the axial velocity amplitudes presented in Fig. 8 have been normalized by the piston velocity amplitude and calculated as a velocity amplitude ratio (β) which can be expressed as;

$$\beta = \frac{\text{Axial velocity amplitude of the liquid medium}}{\text{Velocity amplitude ofthe piston at the particular driving conditions}} \tag{13}$$

The β values at different driving frequencies are presented in Fig. 9. Here, the axial velocity amplitude of the liquid medium is obtained from the PIV measurements and the piston velocity amplitude is calculated as the product of a and ω.

According to Fig. 9, for all the three non-Newtonian fluids, the β values for the first two piston (displacement) amplitude ratios ($A = 0.3$ and 0.4) are almost the same for all the driving frequencies. That implies the absence of nonlinearities in between the first two lower driving amplitudes studied here. However, at higher driving amplitudes, the β values are deviated from the other two, revealing the nonlinearity caused by the shear-thinning of the non-Newtonian fluids. All the experimental cases except a couple of low-frequency cases show an increment of β value with the increased driving frequency.

3.3. Cross-sectional average velocity distribution

As explained by Amaratunga et al. [50], the instantaneous velocity field of a Newtonian fluid has the same sign everywhere within its spatial domain. However, for the non-Newtonian fluids (even for slightly viscoelastic fluids as investigated in this study), the flow resolves into annular regions of alternating upward and downward motion. It is important to know that these annular regions are separated by quiescent boundaries where the shear stress reaches local maxima. This could be easily seen from Fig. 7. Since the velocity distribution of non-Newtonian fluids can take several shapes, either parabolic or the so-called 'Mexican hat type', the individual axial velocity components along the radial distance and also the magnitude of the velocity amplitude do not provide a clear picture about the correct distribution of the velocity across the cross-section. Therefore, a new parameter called the cross-sectional average velocity (V_{ave}) [1] can then be defined for a pipe flow in a circular

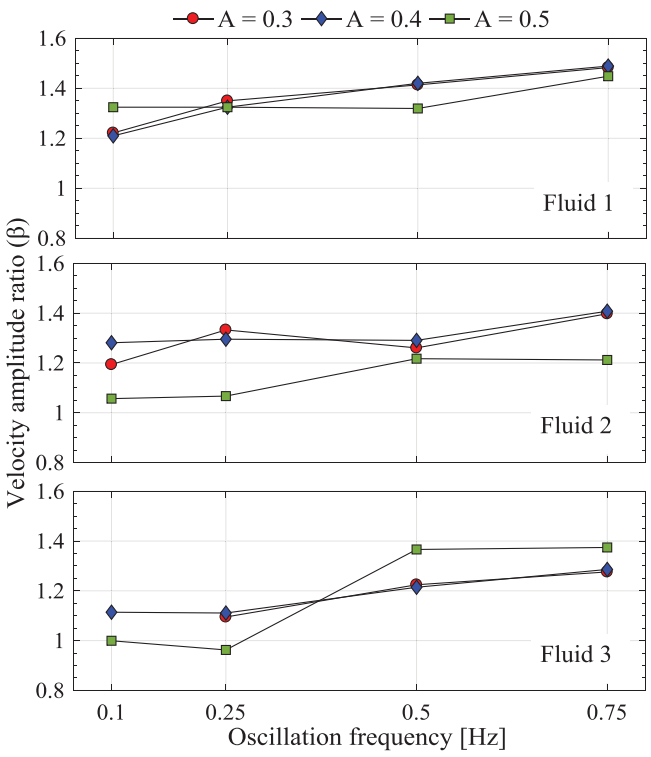

Fig. 9. Velocity amplitude ratio (β) for different non-Newtonian fluids at different oscillating conditions.

cross-section as;

$$V_{ave} = \frac{1}{\pi R^2} \int_0^R V(r).\, 2\pi r.dr \tag{14}$$

where r is the radial position between 0 and R. By calculating the cross-sectional average velocity as given by Eq. (14) it allows us to obtain an indication of how the bulk velocity at that particular moment of time is established both qualitatively (direction-wise) and quantitatively. For instance, even the axial velocity is showing a higher positive magnitude in a case of a non-Newtonian fluid, the magnitude close to the shear region may have achieved two negative peaks in axial velocity which reduces the overall cross-sectional average velocity and results with a lower value. In order to illustrate this better, the instantaneous velocity amplitudes (V) at specific positions of the phase cycle have been normalized by the calculated cross-sectional average velocity (V_{ave}) as;

$$\text{Normalized axial velocity} = \frac{V}{V_{ave}} \tag{15}$$

Fig. 10(a) and (b) show the normalized axial velocity for six different test cases where the phase positions are based on the notation plot presented in Fig. 5. Here, the V_{ave} is calculated based on the instantaneous axial velocities along the radial distance of the pipe.

The normalized axial velocity values of all the six test cases depict the periodical structure of the flow due to the oscillatory motion where $\omega t/(\pi/4) = 2$ and $\omega t/(\pi/4) = 6$ are the closest to unity. It means that at $\omega t/(\pi/4) = 2$ and 6, the instantaneous velocities along the radial direction manifest a profile close to parabolic and they are almost unidirectional without having any alternating upward and downward motions among the small annular regions. According to Fig. 10(a), it can be seen that V_{ave} is increasing and hence the normalized axial velocity is decreasing with the increasing displacement amplitude ratio of the piston for the same fluid type. This could be attributed to a low degree of fullness in its own profile, and deviation from the parabolic shape is considerable at lower piston amplitude ratio (A) values. It can be observed that the magnitude of V_{ave} is increased with increasing frequency

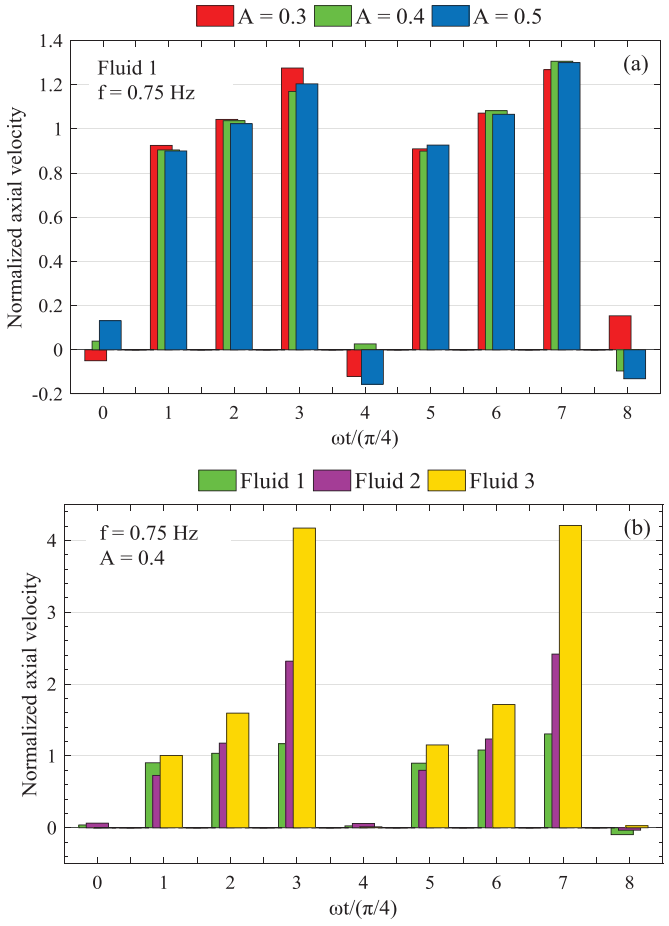

Fig. 10. Comparison of normalized axial velocity at (a) different driving amplitude ratios, but same fluid type (b) different non-Newtonian fluids, but the same driving amplitude.

irrespective of the type of fluid. However, according to Fig. 10(b), it can be further confirmed that, when the flow behavior index (n) value of the non-Newtonian fluid is decreasing, the fluid becomes more viscous and the normalized axial velocity is increasing at all the phase positions for a particular amplitude ratio. The explanation is that when the fluid viscosity and hence friction increases, the uneven distribution of the velocity profile becomes more pronounced. Therefore, V_{ave} becomes lower for the highly viscous fluids compared to that of low viscous fluids, which results in an increment of the normalized axial velocities.

3.4. Variation of the shear rate due to oscillatory motion

One of the main objectives of this study is to investigate how the shear rate is varying in the presence of oscillatory motion. The shear rate was defined in Eq. (10), linked directly to the velocity gradient [57]. It is obvious here that, unlike in conventional unidirectional steady pipe flow, unsteady oscillatory pipe flow undergoes flow reversals continuously and thus the axial velocity is varying both in magnitude and direction. Thus, the shear rate is time-varying and effects from that become more pronounced for non-Newtonian fluids.

In the following section, we try to evaluate and illustrate the impact of the oscillatory motion of a shear-thinning non-Newtonian fluid on the shear rate. Fig. 11 shows how the instantaneous shear rate of Fluid 3 is varying along with the radial position when the fluid undergoes through the different positions of the phase cycle oscillating at $f = 0.75$ Hz and $A = 0.5$. For illustration purpose and brevity, only a single test case has been used for this figure, and the raw experimental

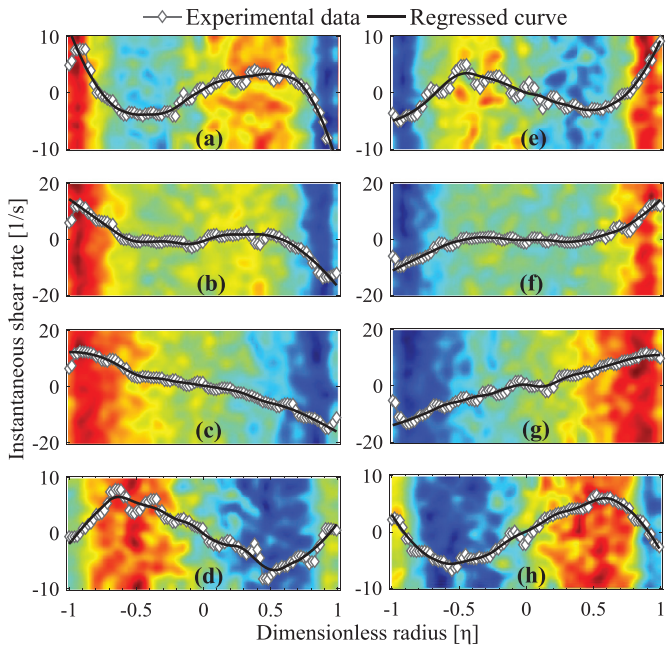

Fig. 11. Change of instantaneous shear rate for Fluid 3 with the phase position at $f = 0.75$ Hz and $A = 0.5$ (a) $k = 0$; (b) $k = 1$; (c) $k = 2$; (d) $k = 3$; (e) $k = 4$; (f) $k = 5$; (g) $k = 6$; (h) $k = 7$ (* The color scale for each subfigure is defined by the magnitude of each plot itself – vertical axis). (For interpretation of the references to color in this figure legend, the reader is referred to the web version of this article.)

data has been regressed with a R^2 value greater than 95% for clarity. The non-dimensional phase position $\omega t/(\pi/4)$ has been denoted as k in the figure caption.

According to the profiles shown in Fig. 11, it can be seen that there is a significant variation in shear rate throughout the pipe cross-section. This is so important to understand with respect to the particle settling/separation point of view since the variation of rate of shear directly affects the viscosity of the shear-thinning non-Newtonian fluids and consequently on the drag reduction. At phase positions where the velocity profiles show some “Mexican hat” type distribution (see Fig. 7), there seem to be two or three points where the change in shear rate becomes zero. The shear rate profiles are even steeper close to the wall regions in such phase positions such as $\omega t/(\pi/4) = 0$, and 4. When the flow reaches to its maximum phase position where $\omega t/(\pi/4) = 2$ or 6, the distribution of the rate of shear seems to show more or less linear profile from the wall to the center region which makes the settling particles in such a system experience differences in viscosity of the fluid medium. However, the maximum change of shear rate is achieved at the maximum position of the phase cycle ($\omega t/(\pi/4) = 2$ or 6), where the axial velocity also possesses the highest magnitude.

The different PIV generated color patterns in the background of the shear rate profiles shown in Fig. 11 illustrate the shear rate magnitudes for a case of $De = 0.078$ and $\delta_{ve} = 18$ mm. The red color (or dark blue color for the opposite direction) indicates the peak shear region and it could be seen that the wall shear tends to propagate towards the pipe centerline through the oscillation cycle. This experimental observation possesses a deviated behavior from the theoretical explanation provided in Section 1.3.4 regarding the definition of ‘wide’ systems as explained by Casanellas and Ortin [55]. This could be attributed specifically to the rheological characterization of the test fluids where they are not pure Maxwellian fluids and also to the highly reversing flow phenomena in the experimental setup. The test fluids were slightly viscoelastic according to Section 3.1. Therefore, they neither behave similar to pure Maxwell fluids nor show the properties of pure Newtonian fluids.

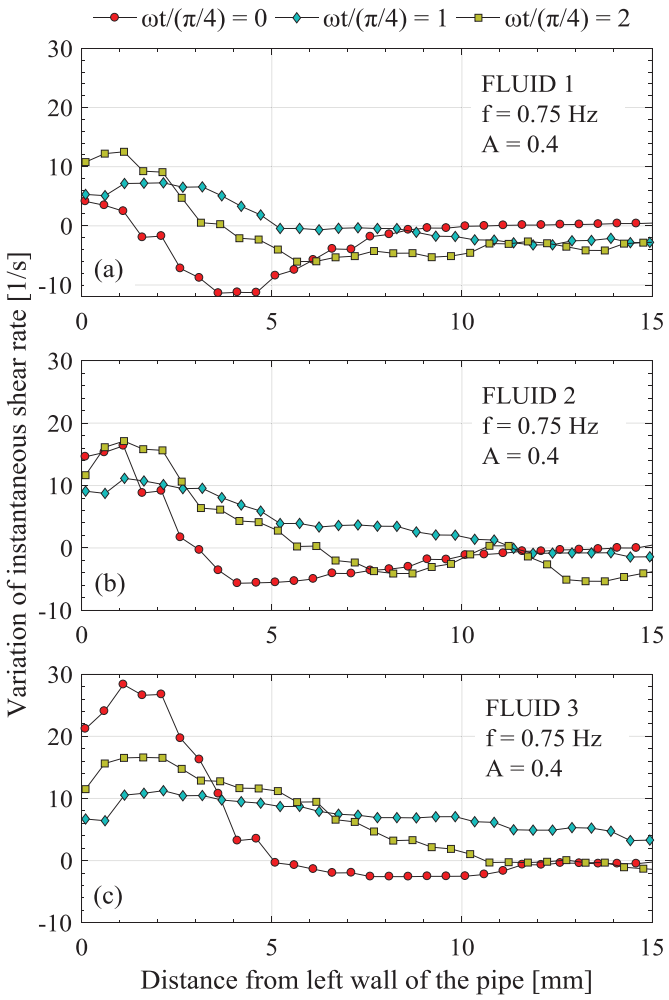

Fig. 12. Instantaneous shear rate profile close to the pipe wall for different non-Newtonian fluids.

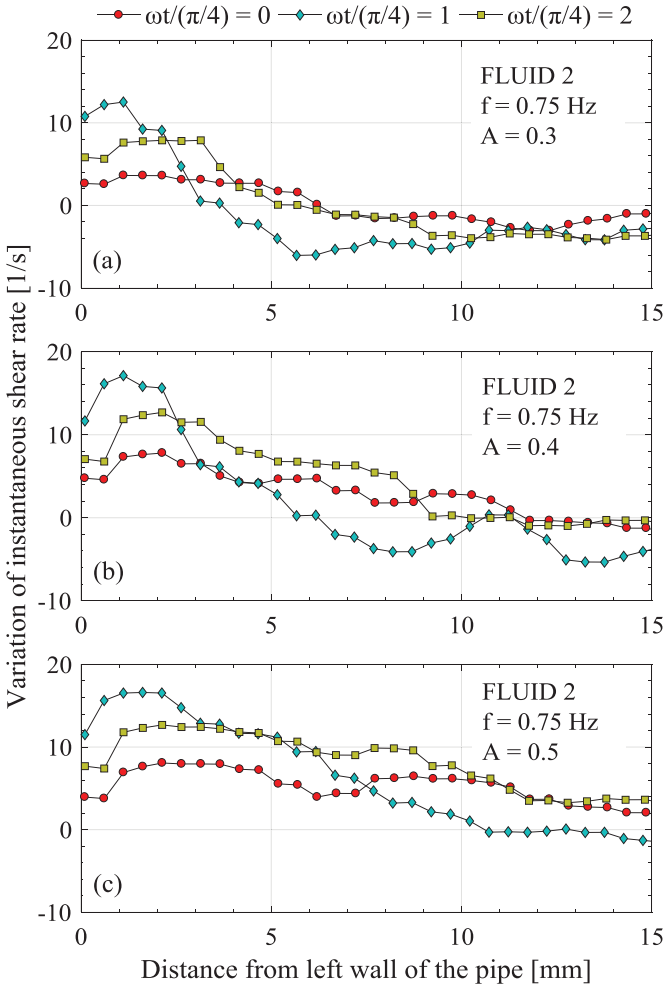

Fig. 13. Instantaneous shear rate profile close to the pipe wall for different oscillation amplitude ratios.

3.4.1. Variation of instantaneous shear rate with different non-Newtonian fluids under different oscillatory conditions

As seen in Fig. 11, the thickness of the shear region is changing through the phase cycle. Since the shear rate change is a key parameter in this study, it is important to check how the shear rate varies with respect to the different non-Newtonian fluids with different viscosities and also with different oscillatory conditions. Fig. 12 illustrates the shear rate profiles with different non-Newtonian fluids with different n values close to the left wall of the pipe, only for three different phase positions.

The shear rate profiles for the presented phase positions in Fig. 12 seem to reach zero with a much shorter distance from the wall for less viscous fluids (with higher n values) compared to that of high viscous fluids (with lower n values). That provides some insight on the thickness of the shear region where it increases with decreasing n value. The thickness of the shear region is estimated by calculating the shear rate from the velocity data obtained from PIV analysis and plotting them in color maps such as shown in Fig. 11. Specifically, at $\omega t/(\pi/4) = 0$, the shear rate variation becomes more significant within the first 5 mm from the wall, for high viscous fluids than that of less viscous fluids. A similar trend could be observed from Fig. 13 which illustrates the shear rate variation close to the left wall of the pipe with different (displacement) amplitude ratios of the piston, only for three different phase positions.

It confirms the fact that the change of shear rate is maximum near the wall region of the pipe. The thickness of the shear region seems to increase with the increasing oscillation amplitude ratio for a particular fluid type. Furthermore, the profile of the shear rate becomes linear with approximately a constant gradient with the increasing oscillation amplitude ratio.

Figs. 12 and 13 show that the influence of the wall (shear layer and resulting shear resistance) on the flow velocity may be considered localized in a near-wall area at a distance of 5 – 10 mm. These shear rate variations greatly affect the viscosity of the oscillating fluid within the pipe and hence influences the solids settling rate significantly.

3.4.2. Predictions on the effect on particle settling/solids control in drilling fluids

Particle settling and solids control is a comprehensive topic when it comes to non-Newtonian fluids for drilling purposes. The removal efficiency of cuttings from the well and also the solids separation efficiency through primary solids control devices are strongly dependent on the properties of the drilling mud that is circulated through the well. According to Saasen and Hodne [45], viscosity profile, gel formation and extensional viscosity of the fluid are the main aspects to this regard. This study also tries to provide a prediction on how viscosity profiles due to the oscillatory motion would influence the particle settling with non-Newtonian fluids. Fig. 14 shows an enlarged section of previously presented viscosity curves of the test fluids in Fig. 2.

It is magnified around $\dot{\gamma} = 100$ 1/s to emphasize the applicability of present experimental results into the practical operating shear rate [65] in a drilling pipe. Based on the shear rate profiles for all the test

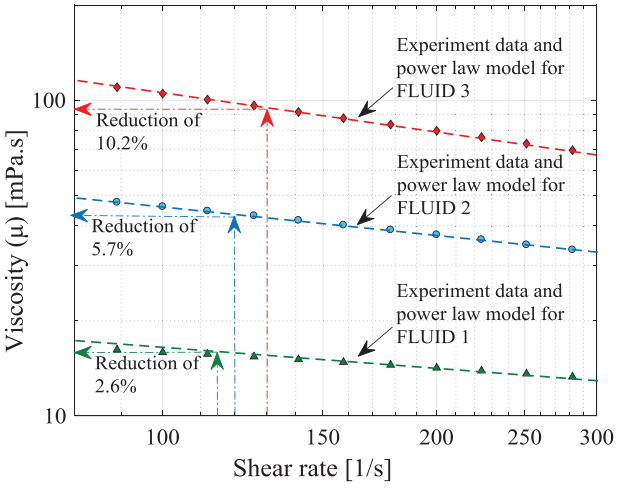

Fig. 14. Illustration of viscosity change due to the variation in shear rate.

cases, the authors have decided to quantify the maximum amount of shear rate change for Fluid 1, Fluid 2 and Fluid 3 to be approximately 15, 20 and 30 1/s respectively. This is slightly less than the reduction approximated by Saasen and Hodne [44] in their experiment, where they have applied the vibration directly to the viscosity measuring cup. With that information, Fig. 14 illustrates how an increment of shear rate (at $\dot{\gamma}$ = 100 1/s) would result in the change in viscosity of the shear-thinning non-Newtonian drilling fluid.

It can be observed from Fig. 14 that a considerable amount of viscosity reduction occurs as a result of the oscillatory motion. The maximum reduction of viscosity has been reported for the most viscous and the least elastic fluid (Fluid 3) and the viscosity reduction becomes insignificant when the non-Newtonian fluids become less viscous. The viscosity of most water-based drilling fluids is formulated by a combination of polymers similar to the test fluids in the current study. In addition, water-based drilling fluids may contain some additives to achieve desired agglomeration effects. However, Saasen and Hodne [45] state that, the structural units and surface charges between those particles in polymeric liquids may get weakened by the oscillations/vibrations and that leads to a reduction of internal liquid viscosity. It is to be noted that the cyclic maximum shear rate change occurs mostly near the pipe wall, and thus the resulting viscosity reduction is more pronounced in the near-wall regions. This explains the fact that, when the shear-thinning non-Newtonian fluids (primarily water-based polymeric liquids) are subjected to oscillatory motion, there will be a substantial reduction of viscosity of the fluid and that will result in the reduction of the drag force on the settling particles and consequently in increased particle settling. It is important to identify that, this increased settling could mostly be expected close to the wall regions and not at the core of the pipe based on the radial shear rate profiles shown in Figs. 12 and 13. This could be contradictory to the typical wall-effects described in many of the particle settling studies performed in quiescent fluid systems. The major difference here is the application of a highly reversing oscillatory flow field and thus a high degree of agitation-disturbance compared to those quiescent Newtonian or non-Newtonian liquid columns.

4. Conclusion

This experimental investigation was carried out to study how the viscous properties of shear-thinning non-Newtonian fluids alter when being exposed to oscillatory conditions. Three different non-Newtonian fluids were tested for four different low frequencies and for three different oscillation amplitudes. The study concludes that;

- PIV is a very good non-intrusive technique to analyze oscillatory flow both for Newtonian and non-Newtonian fluids. It provides insight into the velocity profile at the near-wall regions as well as in the core region. It is fair to say that presently there are no other experimental techniques that can measure velocity profiles with such resolution in space and time. The color maps obtained through PIV analysis are useful in identifying the shear regions and fluctuations in such a study.
- The combined (near wall) shear force and liquid inertia cause the velocity profile to become a complicated radial function quite different from the plug flow imposed by the oscillating piston.
- The thickness of the shear region decreases with increasing oscillation frequency. The axial velocity in the shear region either lags or leads the axial velocity in the central pipe region by a small amount, and tends to be zero at some certain positions of the phase cycle.
- The centerline velocity amplitude increases with increasing frequency and with increasing oscillating amplitude ratio. This is irrespective of the non-Newtonian fluid type.
- With increasing viscosity, the resistance increases and the axial velocity amplitude and V_{ave} reduces. Associated with this the velocity profile becomes more complex and uneven due to the interplay of viscous and inertial forces.
- The change of shear rate is maximum near the wall region and occurs at the maximum position of the phase cycle ($\omega t/(\pi/4)$ = 2 or 6), where the axial velocity is also maximum.
- The shear rate profile becomes linear from the pipe wall to the centerline at the maximum position of the phase cycle ($\omega t/(\pi/4)$ = 2 or 6).
- During low-frequency oscillations, the maximum reduction of viscosity has been reported for the most viscous and the least elastic fluid (Fluid 3). The viscosity reduction becomes insignificant when the non-Newtonian fluids become less viscous.
- The evaluation of the oscillating Reynolds number based on viscoelastic Stokes boundary layer for this particular study revealed that inertia is not responsible for the destabilization of the basic flow and it is basically the viscous forces that dominate within the oscillatory flow system.

Therefore, the presented application of the PIV technique to give velocity distribution and shear rate variation in oscillatory flow in a vertical pipe may bring more detailed information on oscillatory flow characteristics together with a detailed rheological characterization.

Acknowledgment

Authors gratefully acknowledge the Norwegian Research Council for funding this study under the project “NFR Improved Model Support in Drilling Automation”. We appreciate the valuable support provided by Jon Arne Evjenth, from the Department of Energy & Petroleum Engineering at the University of Stavanger in preparing the data acquisition system for the experiments. The advice and encouragement provided by Roar Nybø and Knut S. Bjørkevoll from SINTEF, Bergen are also greatly appreciated.

References

[1] L. Fishler, R. Brodkey, Transition, turbulence and oscillating flow in a pipe a visual study, Exp Fluids 11 (6) (1991) 388–398.
[2] M.Y. Gundogdu, M.O. Carpinlioglu, Present state of art on pulsatile flow theory: part 1: laminar and transitional flow regimes, JSME Int. J. Ser. B Fluids Therm. Eng. 42 (3) (1999) 384–397.
[3] G. Yamanaka, H. Kikura, Y. Takeda, M. Aritomi, Flow measurement on an oscillating pipe flow near the entrance using the UVP method, Exp Fluids 32 (2) (2002) 212–220.
[4] S. Sergeev, Fluid oscillations in pipes at moderate Reynolds numbers, Fluid Dyn. 1 (1) (1966) 121–122.
[5] M. Hino, M. Sawamoto, S. Takasu, Experiments on transition to turbulence in an oscillatory pipe flow, J. Fluid Mech. 75 (2) (1976) 193–207.
[6] M. Ohmi, M. Iguchi, K. Kakehashi, T. Masuda, Transition to turbulence and velocity distribution in an oscillating pipe flow, Bull. JSME 25 (201) (1982) 365–371.
[7] P.R. Hoskins, Estimation of blood velocity, volumetric flow and wall shear rate using Doppler ultrasound, Ultrasound 19 (3) (2011) 120–129.

[8] R.W. Time, A. Rabenjafimanantsoa, On the relevance of laboratory scale rheometric measurements for calculation of complex large scale flows in well drilling and pipe flows, Ann. Trans. Nordic Rheol. Soc. 22 (2013).

[9] S.P. Singh, A.K. Srivastava, J.F. Steffe, Vibration induced settling of a sphere in a Herschel-Bulkley fluid, J. Food Eng. 13 (3) (1991) 181–197.

[10] Y. Su, J.H. Davidson, F. Kulacki, Fluid flow and heat transfer structures of oscillating pipe flows, Int. J. Mech. Aerosp. Ind. Mechatron. Manuf. Eng. 5 (9) (2011) 1813–1822.

[11] A. Aarts, G. Ooms, Net flow of compressible viscous liquids induced by travelling waves in porous media, J. Eng. Math. 34 (4) (1998) 435–450.

[12] A. Lambert, G. Ibáñez, S. Cuevas, J. Del Río, Optimal behavior of viscoelastic flow at resonant frequencies, Phys. Rev. E 70 (5) (2004) 056302.

[13] M.Y. Gundogdu, M.O. Carpinlioglu, Present state of art on pulsatile flow theory: part 2: turbulent flow regime, JSME Int. J. Ser. B Fluids .Therm. Eng. 42 (3) (1999) 398–410.

[14] M. IGUCHI, M. OHMI, K. MAEGAWA, Analysis of free oscillating flow in a U-shaped tube, Bull. JSME 25 (207) (1982) 1398–1405.

[15] D.M. Eckmann, J.B. Grotberg, Experiments on transition to turbulence in oscillatory pipe flow, J. Fluid Mech. 222 (1991) 329–350.

[16] K.H. Ahn, M.B. Ibrahim, Laminar/turbulent oscillating flow in circular pipes, Int. J. Heat Fluid Flow 13 (4) (1992) 340–346.

[17] R. Trip, D. Kuik, J. Westerweel, C. Poelma, An experimental study of transitional pulsatile pipe flow, Phys. Fluids 24 (1) (2012) 014103.

[18] G.B. Thurston, Theory of oscillation of a viscoelastic medium between parallel planes, J. Appl. Phys. 30 (12) (1959) 1855–1860.

[19] G.B. Thurston, Theory of oscillation of a viscoelastic fluid in a circular tube, J. Acoust. Soc. Am. 32 (2) (1960) 210–213.

[20] E. Khabakhpasheva, V. Popov, A. Kekalov, E. Mikhailova, Pulsating flow of viscoelastic fluids in tubes, J. Non Newton. Fluid Mech. 33 (3) (1989) 289–304.

[21] R. Balmer, M. Florina, Unsteady flow of an inelastic power-law fluid in a circular tube, J. Non Newton. Fluid Mech. 7 (2–3) (1980) 189–198.

[22] H. Barnes, P. Townsend, K. Walters, Flow of non-Newtonian liquids under a varying pressure gradient, Nature 224 (5219) (1969) 585.

[23] H. Barnes, P. Townsend, K. Walters, On pulsatile flow of non-Newtonian liquids, Rheol. Acta 10 (4) (1971) 517–527.

[24] A. Siginer, Oscillating flow of a simple fluid in a pipe, Int. J. Eng. Sci. 29 (12) (1991) 1557–1567.

[25] M. Torralba, A. Castrejón-Pita, G. Hernández, G. Huelsz, J. Del Rio, J. Ortín, Instabilities in the oscillatory flow of a complex fluid, Phys. Rev. E 75 (5) (2007) 056307.

[26] P.A. Vasquez, Y. Jin, K. Vuong, D.B. Hill, M.G. Forest, A new twist on stokes' second problem: partial penetration of nonlinearity in sheared viscoelastic layers, J. Non Newton. Fluid Mech. 196 (2013) 36–50.

[27] J. Del Rio, M.L. De Haro, S. Whitaker, Enhancement in the dynamic response of a viscoelastic fluid flowing in a tube, Phys. Rev. E 58 (5) (1998) 6323.

[28] J.A. del Río, M. López de Haro, and S. Whitaker, Erratum: enhancement in the dynamic response of a viscoelastic fluid flowing in a tube [Phys. rev. e 58, 6323 (1998)], Phys. Rev. E, vol. 64, no. 3, p. 039901, 08/27/ 2001, doi:10.1103/PhysRevE.64.039901.

[29] E.E. Herrera, F. Calderas, A. Chávez, O. Manero, Study on the pulsating flow of a worm-like micellar solution, J. Non Newton. Fluid Mech. 165 (3–4) (2010) 174–183.

[30] L. Casanellas, J. Ortín, Experiments on the laminar oscillatory flow of wormlike micellar solutions, Rheol. Acta 51 (6) (2012) 545–557.

[31] S.M. Mitran, M.G. Forest, L. Yao, B. Lindley, D.B. Hill, Extensions of the ferry shear wave model for active linear and nonlinear microrheology, J. Non Newton. Fluid Mech. 154 (2–3) (2008) 120–135.

[32] J.D. Ferry, Studies of the mechanical properties of substances of high molecular weight I. a photoelastic method for study of transverse vibrations in gels, Rev. Sci. Instrum. 12 (2) (1941) 79–82.

[33] J.D. Ferry, Mechanical properties of substances of high molecular weight. ii. rigidities of the system polystyrene-xylene and their dependence upon temperature and frequency, J. Am. Chem. Soc. 64 (6) (1942) 1323–1329.

[34] B.S. Lindley, M.G. Forest, B.D. Smith, S.M. Mitran, D.B. Hill, Spatial stress and strain distributions of viscoelastic layers in oscillatory shear, Math. Comput. Simul. 82 (7) (2012) 1249–1257.

[35] S. He, J. Jackson, An experimental study of pulsating turbulent flow in a pipe, Eur. J. Mech.-B/Fluids 28 (2) (2009) 309–320.

[36] P. Papadopoulos, A. Vouros, Pulsating turbulent pipe flow in the current dominated regime at high and very-high frequencies, Int. J. Heat Fluid Flow 58 (2016) 54–67.

[37] Y.A. Andrienko, D. Siginer, Y.G. Yanovsky, Resonance behavior of viscoelastic fluids in Poiseuille flow and application to flow enhancement, Int. J. Non Linear Mech. 35 (1) (2000) 95–102.

[38] M.F. Letelier, D.A. Siginer, D.L. Almendra, J.S. Stockle, Resonance in laminar pipe flow of non-linear viscoelastic fluids, Int. J. Non Linear Mech. 115 (2019) 53–60.

[39] L. Casanellas, J. Ortín, Vortex ring formation in oscillatory pipe flow of wormlike micellar solutions, J. Rheol. (N Y) 58 (1) (2013) 149.

[40] J. Castrejón-Pita, J. Del Río, A. Castrejón-Pita, G. Huelsz, Experimental observation of dramatic differences in the dynamic response of Newtonian and Maxwellian fluids, Phys. Rev. E 68 (4) (2003) 046301.

[41] D. Tsiklauri, I. Beresnev, Enhancement in the dynamic response of a viscoelastic fluid flowing through a longitudinally vibrating tube, Phys. Rev. E 63 (4) (2001) 046304.

[42] M. Torralba, J. Castrejón-Pita, A. Castrejón-Pita, G. Huelsz, J. Del Río, J. Ortín, Measurements of the bulk and interfacial velocity profiles in oscillating Newtonian and Maxwellian fluids, Phys. Rev. E 72 (1) (2005) 016308.

[43] H.A. Barnes, J.F. Hutton, K. Walters, An Introduction to Rheology, Elsevier, 1989.

[44] A. Saasen, H. Hodne, Influence of vibrations on the rheological properties of drilling fluids and its consequence a solids control, Appl. Rheol. 26 (2) (2016) 28–33.

[45] A. Saasen, H. Hodne, The influence of drilling fluid rheological properties on primary solids control, in: Proceedings of the 34th International Conference on Ocean, Offshore and Arctic Engineering, ASME 2015, American Society of Mechanical Engineers, 2015 pp. V010T11A037-V010T11A037.

[46] L. Børgesson, A. Fredriksson, 32 INFLUENCE of vibrations on the rheological properties of cemenT, in: Proceedings of the International Conference on Rheology of Fresh Cement and Concrete, Liverpool, 1990, CRC Press, 2014, p. 313.

[47] D. Quemada, Rheological modelling of complex fluids. I. THE concept of effective volume fraction revisited, Eur. Phys. J.-Appl. Phys. 1 (1) (1998) 119–127.

[48] M. OHMI, M. Iguchi, Critical reynolds number in an oscillating pipe flow, Bull. JSME 25 (200) (1982) 165–172.

[49] P. Merkli, H. Thomann, Transition to turbulence in oscillating pipe flow, J. Fluid Mech. 68 (3) (1975) 567–576.

[50] M. Amaratunga, H.A. Rabenjafimanantsoa, R.W. Time, Comparison of oscillatory flow conditions in Newtonian and non-Newtonian fluids using PIV and high-speed image analysis, Flow Meas. Instrum. 70 (2019) 101628.

[51] T. Zhao, P. Cheng, The friction coefficient of a fully developed laminar reciprocating flow in a circular pipe, Int. J. Heat Fluid Flow 17 (2) (1996) 167–172.

[52] J. Gerrard, M. Hughes, The flow due to an oscillating piston in a cylindrical tube: a comparison between experiment and a simple entrance flow theory, J. Fluid Mech. 50 (1) (1971) 97–106.

[53] J.R. Womersley, An Elastic Tube Theory of Pulse Transmission and Oscillatory Flow in Mammalian Arteries, Aerospace Research Labs Wright-Patterson AFB OH, 1957.

[54] R.J. Poole, The Deborah and Weissenberg numbers, Rheol. Bull. 53 (2) (2012) 32–39.

[55] L. Casanellas, J. Ortı, Laminar oscillatory flow of Maxwell and Oldroyd-b fluids: theoretical analysis, J. Non Newton. Fluid Mech. 166 (23–24) (2011) 1315–1326.

[56] R.P. Chhabra, J.F. Richardson, Non-Newtonian Flow in the Process Industries: Fundamentals and Engineering Applications, Butterworth-Heinemann, 1999.

[57] M. Amaratunga, R. Nybø, R.W. Time, PIV analysis of dynamic velocity profiles in non-newtonian drilling fluids exposed to oscillatory motion, in: Proceedings of the ASME 2018 37th International Conference on Ocean, Offshore and Arctic Engineering, American Society of Mechanical Engineers, 2018 pp. V008T11A058-V008T11A058.

[58] R.J. Adrian, Particle-imaging techniques for experimental fluid mechanics, Ann. Rev. Fluid Mech. 23 (1) (1991) 261–304.

[59] R. Blythman, T. Persoons, N. Jeffers, D. Murray, Effect of oscillation frequency on wall shear stress and pressure drop in a rectangular channel for heat transfer applications, J. Phys. Conf. Ser. 745 (3) (2016) 032044 IOP Publishing.

[60] J.A. Goshawk, N. Waters, G. Rennie, E. Staples, Enhancement of the drainage of non-Newtonian liquid films by oscillation, J. Non Newton. Fluid Mech. 51 (1) (1994) 21–60.

[61] W. Thielicke, E. Stamhuis, PIVlab–towards user-friendly, affordable and accurate digital particle image velocimetry in MATLAB, J Open Res. Softw. 2 (1) (2014).

[62] K.D. Jensen, Flow measurements, J. Braz. Soc. Mech. Sci. Eng. 26 (4) (2004) 400–419.

[63] T.G. Mezger, The Rheology Handbook: For Users of Rotational and Oscillatory Rheometers, Vincentz Network GmbH & Co KG, 2006.

[64] S.K. Arnipally, E. Kuru, Settling velocity of particles in viscoelastic fluids: a comparison of the shear-viscosity and elasticity effects, SPE J. 23 (5) (2018) 17.

[65] B. Bui, et al., Viscoelastic properties of oil-based drilling fluids, Ann. Trans. Nordic Rheol. Soc. 20 (2012) 33–47.